



Cite this: DOI: 10.1039/d1ee00106j

## Proton selective adsorption on Pt–Ni nano-thorn array electrodes for superior hydrogen evolution activity†

 Adeela Nairan,<sup>‡,a</sup> Caiwu Liang,<sup>‡,a</sup> Sum-Wai Chiang,<sup>a</sup> Yi Wu,<sup>b</sup> Peichao Zou,<sup>ID a</sup> Usman Khan,<sup>c</sup> Wendong Liu,<sup>b</sup> Feiyu Kang,<sup>a</sup> Shaojun Guo,<sup>ID d</sup> Jianbo Wu<sup>ID \*bef</sup> and Cheng Yang<sup>ID \*a</sup>

Conventional acidic water electrolysis for large-scale hydrogen production needs to involve a noble metal catalyst for the anode to resist electrochemical oxidation, while alkaline electrolysis can provide better anode protection, but hydrogen ions become a minority species, which leads to sluggish hydrogen evolution reaction (HER) kinetics. Herein, by developing a unique nano-thorn-like Pt–Ni nano-wire electrode as a superior HER catalyst, we enable a local “pseudo-acidic” environment near the cathode surface in an alkaline electrolyzer. In such a situation, we observed dramatic enhancement of selective H<sup>+</sup> adsorption versus K<sup>+</sup>, leading to an extremely high HER performance towards real applications, with low overpotentials ( $\eta_{\text{geo-surface area}}$ ) of 23 mV and 71 mV at current densities of 10 mA cm<sup>-2</sup> and 200 mA cm<sup>-2</sup>, respectively. This result is exceptionally better than the state-of-the-art Pt-based catalysts in an alkaline electrolyte at large current densities ( $\geq 200$  mA cm<sup>-2</sup>). The simulation result suggests that a strong local electric field around a nano-thorn structure can exponentially increase the diffusion rate of H<sup>+</sup> towards the electrode surface as compared with K<sup>+</sup>, which promotes faster mass transfer and reaction kinetics for the HER in an alkaline medium.

 Received 11th January 2021,  
 Accepted 4th February 2021

DOI: 10.1039/d1ee00106j

[rsc.li/ees](http://rsc.li/ees)

### Broader context

Large-scale production of hydrogen by electrolyzing water is one of the most promising technologies for a future renewable energy society. Conventional acidic water electrolysis requires a noble-metal catalyst at the anode to resist electrochemical oxidation; in alkaline conditions, the plethora of OH<sup>-</sup> is favorable for oxygen evolution and the corrosion issue can be alleviated, but H<sup>+</sup> becomes a minority species, which results in sluggish hydrogen evolution reaction (HER) kinetics at the cathode. In particular, under high current density, H<sup>+</sup> is consumed faster and becomes deficient, and thus the HER is dominated by diffusion control. So, if we can enable a local “pseudo-acidic” environment near the cathode surface in an alkaline electrolyzer, then we can achieve high performance HER for a longer term at high-working-current when involving a cheap metal oxide/hydroxide anode catalyst. Here, we report an exceptionally active and durable HER catalyst based on the hierarchical nano-thorn NiPt structure, which can concentrate the strong localized electric field at the tips and can alter the adsorption kinetics towards different cation species, showing an extremely low overpotential of 71 mV at the current density of 200 mA cm<sup>-2</sup>. This work distinguishes a giant leap for hydrogen generation in alkaline electrolyzers with almost the same efficiency as it evolved from protons in an acidic medium.

<sup>a</sup> Institute of Materials Research, Tsinghua Shenzhen International Graduate School, Tsinghua University, Shenzhen 518055, China. E-mail: yang.cheng@sz.tsinghua.edu.cn

<sup>b</sup> State Key Laboratory of Metal Matrix Composites, School of Materials Science and Engineering, Shanghai Jiao Tong University, 800 Dongchuan Road, Shanghai 200240, China. E-mail: jianbowu@sjtu.edu.cn

<sup>c</sup> Shenzhen Geim Graphene Center, Tsinghua-Berkeley Shenzhen Institute, Tsinghua University, Shenzhen 518055, China

<sup>d</sup> College of Engineering, Peking University, No. 5 Yiheyuan Road, Haidian District, Beijing, 100871, China

<sup>e</sup> Center of Hydrogen Science, Shanghai Jiao Tong University, 800 Dongchuan Road, Shanghai 200240, China. E-mail: jianbowu@sjtu.edu.cn

<sup>f</sup> Materials Genome Initiative Center, Shanghai Jiao Tong University, 800 Dongchuan Road, Shanghai 200240, People's Republic of China. E-mail: jianbowu@sjtu.edu.cn

† Electronic supplementary information (ESI) available. See DOI: 10.1039/d1ee00106j

‡ These authors contributed equally.

# 1 Introduction

As a promising energy carrier, hydrogen has a high energy density, and clean and sustainable characteristics, and is considered as one of the main alternatives to the diminishing fossil fuels.<sup>1–3</sup> It is critically important to develop highly active electrocatalysts to accelerate the reaction kinetics both for the hydrogen evolution reaction (HER) and oxygen evolution reaction (OER). Developing alkaline water electrolysis is of particular importance,<sup>4</sup> as less pricey catalysts (instead of the precious metal) can be involved for the anode without acidic corrosion. Yet for the cathode, lower H<sup>+</sup> concentration leads to more sluggish HER kinetics,<sup>5,6</sup> resulting in two to three orders of magnitude lower HER activity than in acidic solution.<sup>7–9</sup> Such a situation leads to low efficiency in both water-alkali and chloro-alkali electrolyzers as well.<sup>10,11</sup> A key challenge is that even though the hydrogen ions in alkaline solution are a rare species, they can critically determine the number of  $H_{\text{ad}}$ , which is essential for the Volmer step for the HER. Therefore, if it is possible to enable a “pseudo acidic” environment at the cathode, which means more hydrogen ions are accumulated around the electrode surface, the HER kinetics near the catalyst surface can be significantly promoted while maintaining the competitive features for alkaline electrolysis (*e.g.*, low OER catalyst cost and fast OER kinetics), which is critically important for a full electrolyzer. However, there are still other cationic species in the electrolyte, so how to ensure the selective accumulation of H<sup>+</sup> (hydrogen ion) around the cathode surface remains a key challenge to address hereby.

Some recent studies reported that the distribution of electric fields on the electrode surface can significantly alter electrocatalytic performance, particularly related to the CO<sub>2</sub> reduction.<sup>12,13</sup> Liu *et al.* proposed a strategy that can lead to a high concentration of CO<sub>2</sub> at the active sites of the Au electrode.<sup>14</sup> Finite element analysis revealed that the concentrated electric field can attract more K<sup>+</sup>, which is conducive to the reduction of CO<sub>2</sub>, demonstrated by a single nano-needle-structure model. Yet for the HER in the alkaline solution, highly accumulated alkaline metal cations (dominant species) around the cathode surface would compete for the adsorption of hydrogen (rare species); such a situation is unwelcomed in conventional understanding. However, noteworthy, as the hydrogen ion has a lower mass/charge ratio than alkaline metal cations, we may expect that in certain circumstances by rationally designing the electrode architecture, hydrogen ions can become a competitive species for adsorption driven by an electric field and thus alter the catalytic kinetics. Mechanism studies regarding such conditions may provide insights for designing future novel high-performance catalytic electrodes in simple ways, but has not been investigated yet.

Herein, for the first time, we report the scalable preparation of a hierarchical structure featuring Ni nano-thorn-arrays (Ni NTAs) conformally decorated by Pt nano-islands, *via* a unique self-limiting magnetic-field-driven growth technology. Interestingly, the fabricated electrode significantly improves the selective H<sup>+</sup> adsorption on the catalyst surface, which in turn allows us to treat the HER in a “pseudo acidic” local environment by leading the unprecedented catalytic performance in alkaline conditions.

The highly branched electrode architecture possesses an open-porous and thorn-shaped structure consisting of a large number of high curvature surfaces, which can serve as electrochemically active sites and facilitate fast electron transfer during the HER. It is worth mentioning that in comparison with typical smooth Ni nanowire arrays (Ni NWAs), the nano-thorn (NT) structure at the nanowire (NW) surface can provide abundant acute geometry at the nanoscale, which is very favorable to concentrate the localized electric field at tips and provide enhanced H<sup>+</sup> adsorption. Our simulation results show that the concentrated electron on the tips strengthens the adsorption of hydrogen ions, therefore, enhancing the HER kinetics. In addition, the advantage of accelerating H<sup>+</sup> diffusion by our material becomes more pronounced with even higher working current density ( $\geq 200 \text{ mA cm}^{-2}$ ), which will be effective for industrial electrolyzers.

## 2 Results and discussion

### 2.1 Fabrication of the Pt–Ni NTA structure

The detailed fabrication process of Pt–Ni NTAs is illustrated in Fig. 1a. In brief, it involves two main steps. Firstly, the Ni NTAs were grown on a piece of titanium foil *via* a modified magnetic-field-driven growth process; then, a thin Pt layer was electro-deposited on the surface of Ni NTAs (see the details in ESI<sup>†</sup>). Temperature-dependent experiments were conducted, so as to investigate the growth mechanism of the thorn-shaped Ni NTAs (Fig. S1f, ESI<sup>†</sup>). Available studies disclosed the growth mechanism of metallic nanoparticles characterized with nano-star and urchin-like structures prepared by wet chemical methods.<sup>15–17</sup> Delicate control of thermodynamics and capping agent species can lead to unique surface features which are different from many frequently-investigated nanoparticles such as octahedrons, polyhedrons, and polypods.<sup>15–17</sup> Here for the first time, we report a unique three-dimensional hierarchical nanostructure, featuring a bimetallic NTA structure, which is based on a magnetic-field-assisted scalable chemical reduction strategy and surface modifications.

The thorn-shaped structure obtained at 80 °C was selected as an optimized electrode for electrodepositing Pt due to its uniform NTA structure and moderate diameter. The specific surface area of this sample is measured to be  $6 \text{ m}^2 \text{ g}^{-1}$ , based on the Brunauer–Emmett–Teller (BET) analysis (Fig. S2, ESI<sup>†</sup>). The fabricated electrode with a large accessible surface area is expected to improve the HER kinetics by effectively increasing the active electrocatalytic sites and reducing the impedance for the diffusion of the reactants to reach the active sites within the electrode.<sup>18</sup> Thus, the pristine thorn-shaped Ni NTAs combine the advantages of both well-defined surface structure and a large number of catalytic active sites, which are critically important towards high-performance electrocatalysis with improved activity. After electrodepositing a thin layer of Pt atoms, the catalytic property can be drastically improved.

### 2.2 Crystal structure and composition

Scanning electron microscopy (SEM) studies show that the length and diameter of the Ni NWs are about 2 mm and

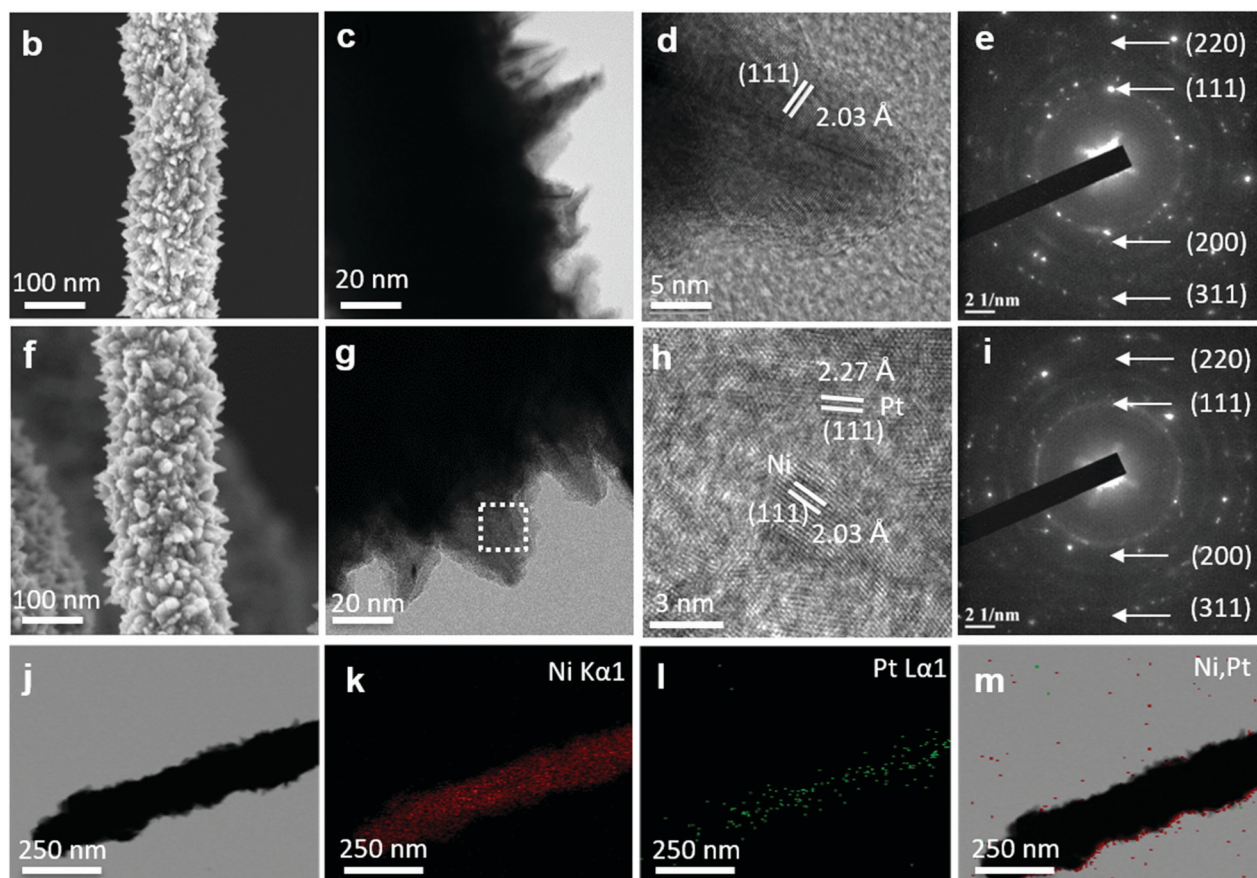
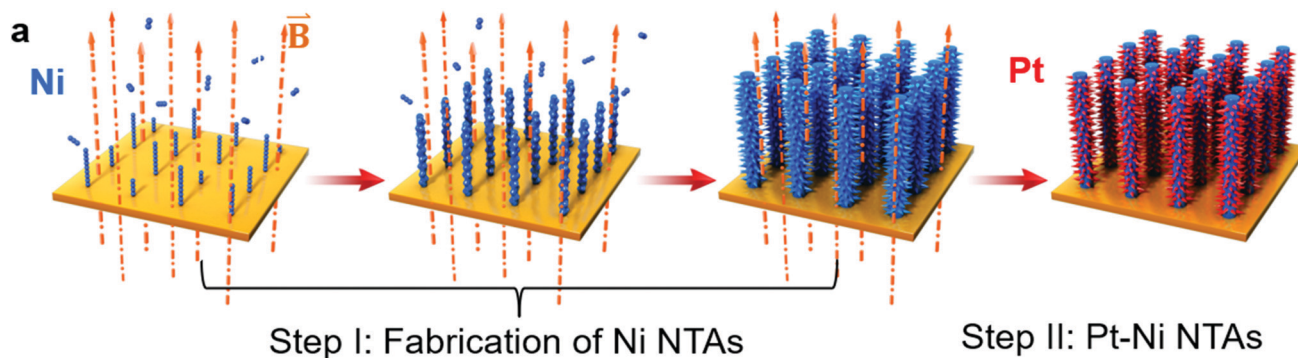


**Fig. 1** Schematic illustration of the fabrication of Pt–Ni NTAs and morphological analysis. (a) Schematic description of the fabrication process for the NT structure through a magnetic field-assisted growth process at varying synthesis temperatures (60 °C, 70 °C, and 80 °C), where the orange dotted lines represent the applied magnetic field: Step I shows the fabrication of Ni NT structures through temperature-controlled experiments. Step II shows Pt deposition (in red color) to form Pt–Ni NTAs with NT geometry. (b) HR-SEM image of a single Ni NT, representing NT geometry. (c) TEM image of the Ni NT structure. (d) HR-TEM image of Ni NT. (e) The corresponding SAED pattern of Ni NT. (f) HR-SEM image of a single Pt–Ni NT, representing NT geometry preserved after electrodeposition. (g) TEM image of single Pt–Ni NTs. (h) HR-TEM image of Pt–Ni NTs showing exposed Pt and Ni planes. (i) SAED pattern of a Pt–Ni NT. (j) HAADF image of an individual Pt–Ni NT. (k–m) The corresponding EDX elemental mapping images of typical Pt–Ni NTs.

350 nm, respectively (Fig. S3a,b, ESI<sup>†</sup> and Fig. 1e). In addition, each branch of Ni NW has a unique NT structure with a tip angle ranging from 40° to 55° on the surface of the NW, which resembles thorns (Fig. S1f, ESI<sup>†</sup>). After depositing a thin Pt layer on the Ni NTs *via* an electrodeposition process, the SEM and transmission electron microscopy (TEM) images indicate that the Pt–Ni NTAs can still maintain their unique morphology

with a high density of sharp NTs (Fig. S4, ESI<sup>†</sup>), which lays the foundation for improving electrocatalytic properties.

The high-resolution SEM and TEM images of a single pristine Ni NT display an abundant number of thorn-like structures on the surface (Fig. 1b and c). The HR-TEM image (Fig. 1d) shows the clear lattice fringes with an inter-planar spacing of 2.03 Å, corresponding to the (111) plane of Ni.

Moreover, the selected area electron diffraction (SAED) pattern was well indexed to the (111), (200), (220) and (311) planes of Ni (Fig. 1e), which is consistent with the XRD analysis of Ni NTs (Fig. S5, ESI<sup>†</sup>). Fig. 1f and g depict the SEM and TEM images of a single NW after electroplating Pt, indicating that these NWs nicely maintain their original one-dimensional morphology with a unique NT surface. The HR-TEM image further confirms the existence of both Pt and Ni elements on the thorns (Fig. 1h). In addition, the representative EDX elemental mapping and line scanning of Pt–Ni NTAs show that both Ni and Pt atoms are distributed over the whole NT surface with an atomic ratio of  $\sim 99.4:0.6$  (Fig. 1j–m, Fig. S6 and S7, ESI<sup>†</sup>), which is close to the inductively coupled plasma atomic emission spectroscopy (ICP-AES) results of 99.8:0.2 (Table S1, ESI<sup>†</sup>). The crystalline phase and chemical composition of both pristine Ni NTAs and Pt–Ni NTAs were also surveyed by X-ray diffraction (XRD) and

X-ray photoelectron spectroscopy (XPS) respectively, as summarized in Fig. S8–S10 (ESI<sup>†</sup>). The XPS results indicate the existence of both Ni and Pt metals on the Pt–Ni NTA surface.<sup>19</sup>

### 2.3 Electrocatalytic HER performance

The HER performances of pristine Ni NTAs and Pt–Ni NTAs and Pt/C (20 wt%, 500  $\mu\text{g cm}^{-2}$ ) were evaluated using linear sweep voltammetry (LSV) curves which were obtained at a low scan rate of 1  $\text{mV s}^{-1}$  in 1 M KOH solution at room temperature (Fig. 2a). The pristine Ni NTAs exhibit a low overpotential of 51 mV at a geometric current density of 10  $\text{mA cm}^{-2}$ , which is a good performance for pure nickel catalysts. Remarkably, Pt–Ni NTAs show an ultra-low overpotential of 23 mV at 10  $\text{mA cm}^{-2}$  and exhibit a super low overpotential of 71 mV to achieve an industrial-level high current density of 200  $\text{mA cm}^{-2}$ , which are significantly lower than those of commercial Pt/C catalysts

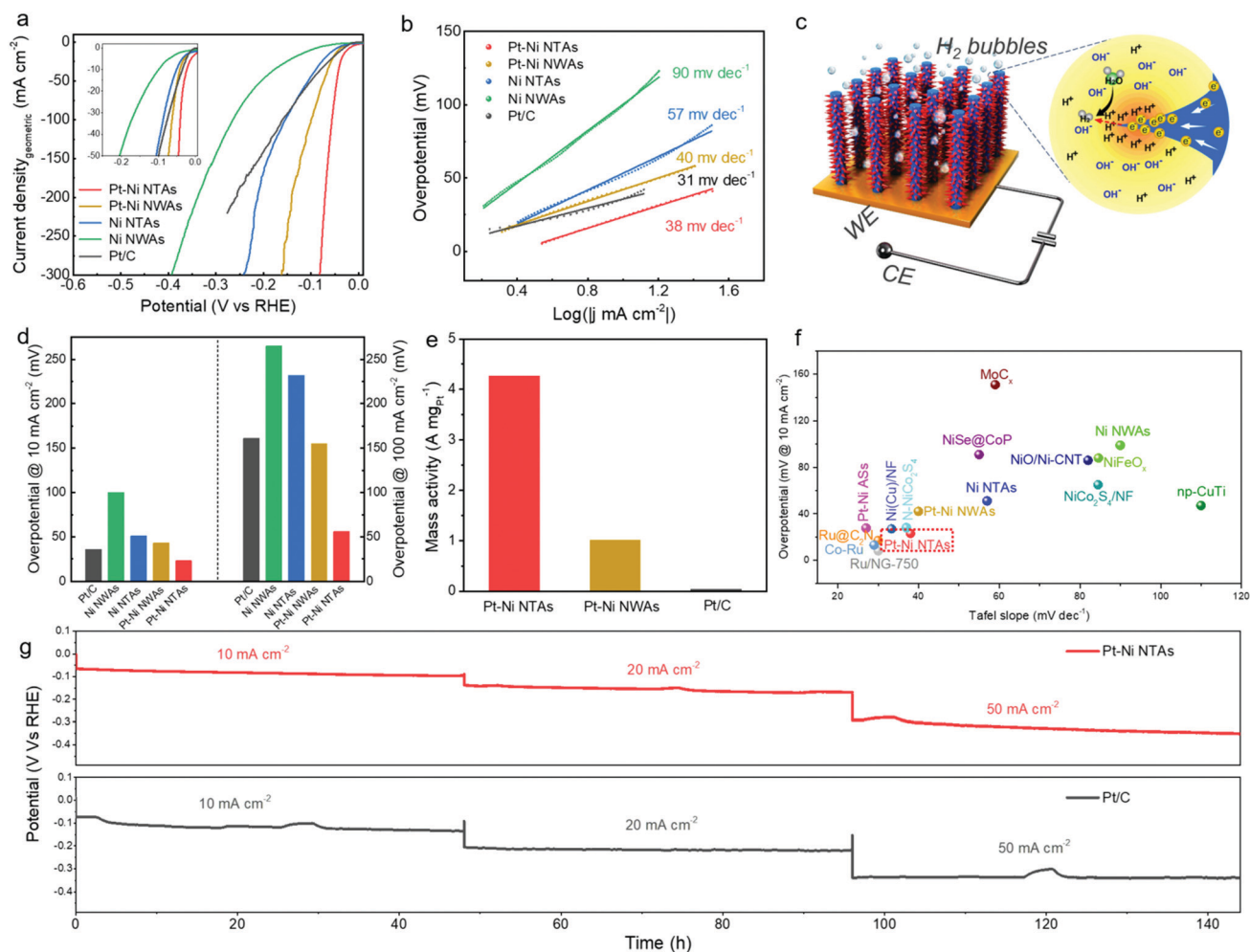


**Fig. 2** Electrocatalytic activities of different electrodes in alkaline medium. (a) HER polarization curves with a scan rate of 1  $\text{mV s}^{-1}$  in 1.0 M KOH solution. Inset: The enlarged details at current densities below 50  $\text{mA cm}^{-2}$ . (b) Tafel plots are derived from the corresponding polarization curves. (c) Schematic illustration of the surface chemistry of Pt–Ni NTAs as the working electrode during electrolysis, an enlarged view of a single NT structure showing the electrochemical field generation on the tip surface (orange color), which will accumulate electrons around the tip and then result in gathering more hydrogen ions through the double-layer effect in the solution, thus accelerating the HER reaction. (d) Overpotentials at a current density of 10  $\text{mA cm}^{-2}$  (left) and 100  $\text{mA cm}^{-2}$  (right). (e) Mass activities of Pt–Ni NTAs, Pt–Ni NWAs and commercial Pt/C at an overpotential of 50 mV and (f) overpotentials and Tafel slope comparison of fabricated Pt–Ni NTAs and Ni NTAs electrodes with other recently reported HER electrocatalysts in 1.0 M KOH solution and (g) chronopotentiometry test at current densities of 10, 20 and 50  $\text{mA cm}^{-2}$  in 1 M KOH solution for 144 h.

(36 mV at 10 mA cm<sup>-2</sup> and 259 mV at 200 mA cm<sup>-2</sup>), and superior to most of the recently reported state-of-the-art HER catalysts (Fig. 2f and Table S2, ESI†). Furthermore, to demonstrate the facilitation of catalytic reactions arising from the NTs on the NW surface, the Ni NWAs and Pt–Ni NWAs with smooth surfaces fabricated by the same process were also evaluated (see the morphology of Ni NWAs in Fig. S11, ESI†). As shown in Fig. 2a, the Ni NWAs and Pt–Ni NWAs show an overpotential of 100 mV and 43 mV at a current density of 10 mA cm<sup>-2</sup>, respectively, which is 49 mV and 20 mV higher than the overpotential for their corresponding NTA structure catalysts. In addition, the activity advantage of the NTA structure becomes more pronounced at higher current densities, and the observed overpotentials of the fabricated electrodes at different current densities are shown in Fig. 2d. The Tafel plots were obtained by fitting the experimental data using the Butler–Volmer equation (Fig. 2b). The Tafel slope of the Pt–Ni NTAs is 38 mV dec<sup>-1</sup>, which is lower than that of the Pt–Ni NWAs (40 mV dec<sup>-1</sup>) and most previously reported HER electrocatalysts (Fig. 2f and Table S2, ESI†), and comparable to Pt/C (31 mV dec<sup>-1</sup>). The Tafel slope of Ni NTAs is also lower than that of Ni NWAs. The low Tafel slope of Pt–Ni NTAs indicates that the recombination of chemisorbed hydrogen atoms on the surface of the catalyst is the rate-determining step and HER reaction kinetics is followed by Volmer Tafel<sup>20</sup> (Fig. 2c). With a low Tafel slope, the HER rate of the fabricated electrode will increase rapidly with increasing overpotential, leading to a competitive advantage for practical applications.

Furthermore, the mass activity for the Pt–Ni NTAs, Pt–Ni NWAs and commercial Pt/C samples was calculated by normalizing the current density with respect to their Pt mass loading at the same overpotential of 50 mV (Fig. 2e). Noticeably, the Pt–Ni NTAs structure exhibits about 4.2 times higher mass activity as compared to Pt–Ni NWAs, (*i.e.*, 4.27 A mg<sub>Pt</sub><sup>-1</sup> over 1.01 A mg<sub>Pt</sub><sup>-1</sup>), and around 100 times higher than commercial Pt/C catalysts (0.043 A mg<sub>Pt</sub><sup>-1</sup>). This indicates that Pt–Ni NTAs can maximize the utilization and catalytic activity of Pt, allowing significant cost reduction for Pt based HER catalysts.

The long-term stability is another critical factor for practical HER applications. Fig. 2g presents the stability test result of the prepared Pt–Ni NTAs recorded at three constant current densities of 10, 20 and 50 mA cm<sup>-2</sup> in alkaline solutions for a total of 144 hours. As shown in Fig. 2g, the as-prepared Pt–Ni NTAs show relatively good stability, with only a 28, 31 and 60 mV increase for overpotentials at 10, 20 and 50 mA cm<sup>-2</sup>, respectively, for a long period of 144 hours. For the Pt/C catalysts, the activity is stable in the first 2 hours and then shows a significant activity decrease, with an overpotential increase of 62 mV within 48 hours at 10 mA cm<sup>-2</sup>. After the first period of 48 hours, the Pt/C became stable again for the rest of the stability test, which might be attributed to the irreversible agglomeration of Pt nanoparticles driven by Ostwald ripening in the first period of the stability test.<sup>21</sup> After the stability assessment for Pt–Ni NTAs, the morphology and composition analyses were examined through SEM and XPS (Fig. S12 and S13, ESI†). Interestingly, the SEM images of Pt–Ni NTAs show that the unique surface morphology is well

maintained. Additionally, the high-resolution XPS spectrum for the Ni 2p<sub>1/2</sub> binding energy exhibits a slight shift towards a high value (~0.4 eV), while the Pt 4f spectrum gradually shifts to lower binding energies (~0.38 eV) after the long-term stability test (Fig. S13, ESI†). Previous studies have demonstrated that the Pt binding energy varies with the adsorption of the adsorbate on the Pt surface, which is determined by the number of low coordination sites in such geometry.<sup>22</sup> These results also indicate the strong interaction between Ni and the deposited Pt on the surface.

Contact angle measurement was also conducted to probe the wettability of the fabricated electrodes by dropping 1.0 M KOH aqueous solution (Fig. S14, ESI†). This result indicates the super-hydrophilic nature of the surface of the prepared electrode towards alkaline solutions, which is attributed to the unique surface feature of NTA,<sup>23</sup> and beneficial for liquid electrolyte transfer. In addition, to compare the size distributions and the dynamics of the hydrogen bubble release on the surface of the fabricated electrodes, we captured the digital photographs of bubble releasing behavior at a current density of 10 mA cm<sup>-2</sup> and 200 mA cm<sup>-2</sup> (Fig. S15, ESI†). It is observed that for the case of Pt–Ni NTAs at large current density, ~85% of hydrogen bubbles smaller than 65 μm leave the surface of the electrode, leading to the constant exposure of catalytic sites to the surrounding electrolyte. Thereby, the fast release of gas bubbles on the surface of Pt–Ni NTAs confirms that this electrode facilitates the mass transfer and HER reaction kinetics.

#### 2.4 Investigation of the origin of enhanced electrocatalytic activity

From the above investigations, it is clear that the pure nickel NTAs show far better HER activity than the smooth pure nickel NWAs. It should be noted that the Ni NTA and Ni NWA samples are both fabricated by the same protocol. From the SEM figures (Fig. S1 and S11, ESI†), the main difference between these two samples is their morphology (*i.e.* with or without nanotips on the nanowire surface). To confirm the “nanotip enhanced effect” on the HER activity, we further eliminate the influence of the different surface area caused by different morphologies of these two samples by comparing their intrinsic activity. Specifically, the electrical double-layer capacitance ( $C_{dl}$ ) of the samples was first measured by cycling the electrode in the non-faradaic regions (Fig. S16, ESI†). The calculated  $C_{dl}$  of Ni NTAs and Ni NWAs is about 10.2 and 4.0 mF cm<sup>-2</sup>, respectively (Fig. 3a). The  $C_{dl}$  normalized polarization curves were utilized to estimate their intrinsic activity. As shown in Fig. 3b, the Ni NTAs exhibit significantly enhanced intrinsic activity compared with the Ni NWAs. Correspondingly, after the deposition of a thin layer of Pt on the surface, Pt–Ni NTAs were also found to exhibit higher intrinsic activity than Pt–Ni NWAs. These electrochemical experiments indicate that in addition to the extra electrochemically active area brought by the high curvature nanotips on the surface of the nanowires, other factors altered the intrinsic HER activity in the Ni NTAs. Previous studies have shown that high curvature structures, *e.g.*, nano-needle or nano-cones benefitting from the strong local electric field can concentrate more positively charged cations and also promote

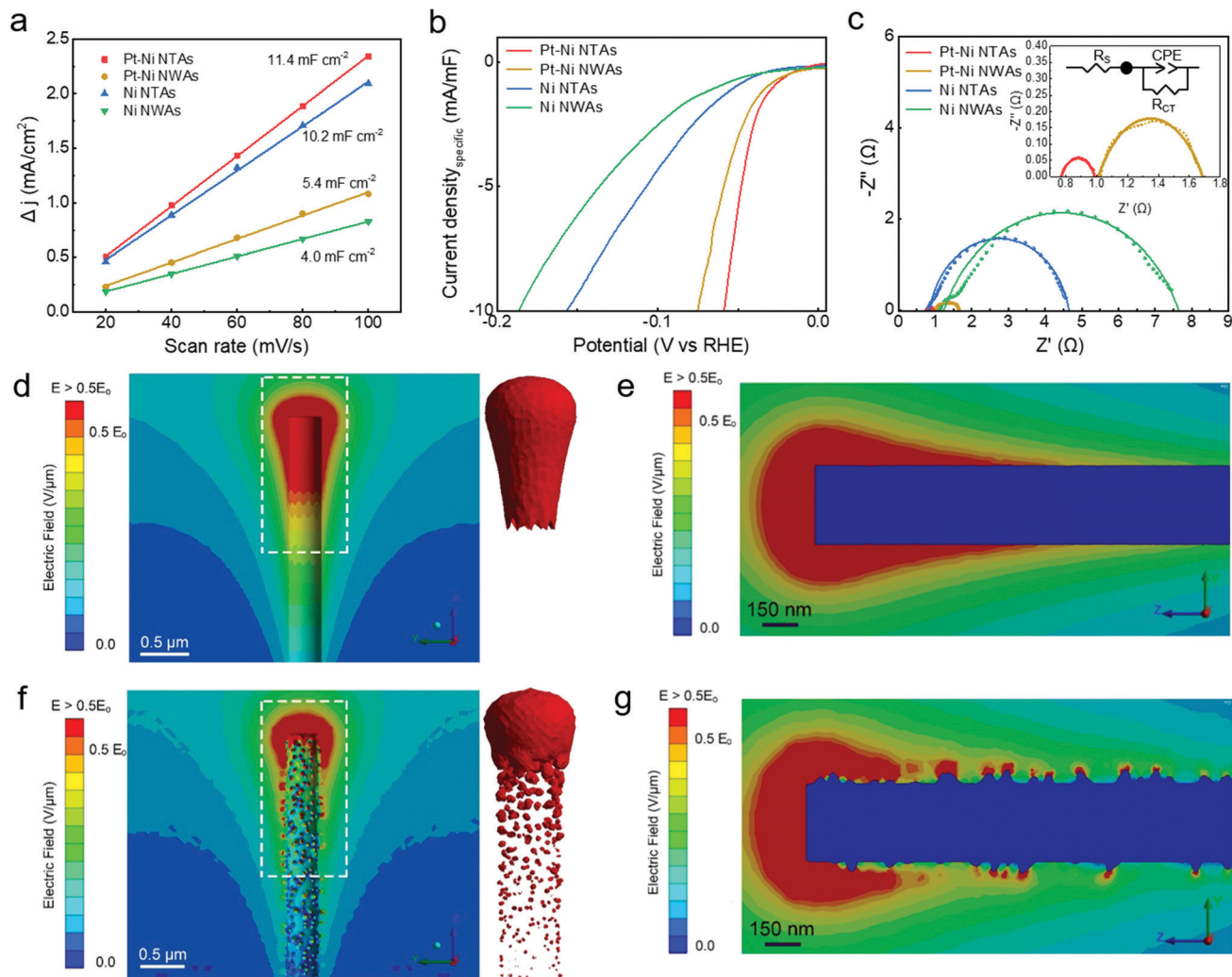


**Fig. 3** Investigation of the electrochemical properties and activity enhancement by local electric field generation on the fabricated electrode. (a) Obtained electrochemical double-layer capacitance ( $C_{dl}$ ) of different electrodes. (b)  $C_{dl}$  normalized polarization curves. (c) Charge transfer resistance analyses. Nyquist plots in 1.0 M KOH electrolyte. (d) The magnification of the electric field is taken from the Z–Y cross-section plane and NW surface. The smooth NW (control case) and corresponding iso-surface showing the iso-volume with electric field value. (e) Magnified picture showing the electric field intensity around the NW surface. (f) NWs decorated with NTs and their corresponding iso-surface showing the iso-volume with high electric field value. (g) Magnified picture showing the locally enhanced electric field intensity around the NW with NTs.

the nucleation of smaller gas bubbles.<sup>12,14,24</sup> Herein, we proposed that the locally enhanced electrostatic field around the abundant high curvature nanotip structure in the Ni NTAs may significantly increase the diffusion rate of  $H^+$  towards the electrode surface and aggregate more  $H^+$  on the surface compared with the situation on smooth Ni NWAs, which leads to a faster mass/charge transfer and reaction kinetics for the HER in alkaline medium and higher intrinsic HER activity. To probe charge transfer processes occurring at the electrode/solution interfaces, we also compared the electrochemical impedance spectra between the NTA samples and NWA samples (Fig. 3c and Table S3, ESI<sup>†</sup>). The semicircle diameter of the Nyquist plot for the NTAs sample is much smaller than their corresponding NWA ones, which reflects an acceleration of the charge transfer process offer by a high curvature nanotip structure.<sup>25,26</sup> In addition, we explore the electrochemical activity of Pt–Ni NTAs and Pt–Ni

NWAs in acidic conditions (0.05 M  $H_2SO_4$ ) and found that the NTA structure still exhibits higher intrinsic activity than the NWA structure, which further confirms the nanotip enhanced effect (Fig. S17, ESI<sup>†</sup>).

To verify the effect of the locally enhanced electrostatic field on the surface of a NW, we employed the widely used finite element simulation packages ANSYS and COMSOL to explore the distribution of electric fields on the NTA and smooth NWA structures. Using the statistics listed in Table S4 (ESI<sup>†</sup>), the model is created with the Monte Carlo generation mechanism. Initially, a single NW model with an NT structure was built up for simulation (Fig. S18, ESI<sup>†</sup>). For a better understanding of the enhanced catalytic property of the active sites, we included the 2D and 3D models representing the electric field distribution on the surface of the NW with thorn structures and a smooth NW as the control case (Fig. S19, ESI<sup>†</sup> and Fig. 3d–g), both of

which are vertically placed in the electric field for modeling. As shown in Fig. 3d and e, for the smooth NW case, a high electric field only occurs near the tips of the NW. Yet for the case of NWs with thorn-like structures, we observe that the sites with high electric field values (red spots in the figures) spread out for larger areas along the NW, instead of only concentrating at the top end of the NW (Fig. 3f and g). These scattered “hot spots” around the cathode area can significantly alter the reaction kinetics at the tip areas, which is believed to be the major driving force in enhancing the catalytic activity. A plausible explanation is that the electric field at the tip areas is drastically enhanced by the high geometric curvature, featured with a great number density of the NTs along the whole NW ( $\sim 140$  per unit  $\mu\text{m}^{-2}$ ). In this way, these highly reactive spots can greatly increase the reactive area along the NW. This phenomenon strongly supports that this unique NT geometry can increase the catalytic activity by widening the distribution of high electric field on the NW, and also strengthens the electric field at the NTs to become highly reactive spots. Accordingly, at the solid side of the electric double layer adjacent to the tip areas, hydrogen ions can be significantly accumulated and hydroxyl ions will be repelled (schematically illustrated in Fig. 2c), which is especially meaningful in the case of alkaline solution, as hydrogen ions only show a small portion in the solution.

Based on the electric field information calculated above, we created another single tip finite element model, which features a much higher lattice element number, so as to calculate the concentration distribution of charged ions in the electrolyte solution under the action of the electric field of the fabricated NW electrode. Based on Maxwell equations, a double layer model was established, using the Gouy–Chapman–Stern theory, to obtain the hydrogen ion and potassium ion concentration distributions on the NT structure in an electrolyte solution. In such a quasi-static simulation condition, the electric field can reach several hundred  $\text{V } \mu\text{m}^{-1}$  in the regions near the Helmholtz layer. Fig. 4a shows that for the NT structure, as the electric field intensity increases from  $100 \text{ V } \mu\text{m}^{-1}$  to  $700$ , the accumulation rate of hydrogen ions is far higher than that of potassium ions in the region  $2 \text{ nm}$  away from the surface. In contrast, the accumulation rate of both ions is almost similar to the case of the smooth NW model (Fig. 4b). To comprehensively compare the change of ion concentration for different structures, we further calculated the hydrogen ion and potassium ion concentrations at different distances to the electrode surface at a certain electric field strength of  $350 \text{ V } \mu\text{m}^{-1}$ . As shown in Fig. 4c, at the point around  $1 \text{ nm}$  to the electrode surface, the hydrogen ion concentration for the NT structure increases by around 2 times, while the value for the smooth structure only increases by around 0.25 times. Therefore, the increase in hydrogen ion concentration for the NT structure is about  $2/0.25 = 8$  times that of the smooth structure. To note, at positions closer to the electrode surface (*e.g.*  $<0.5 \text{ nm}$ ), this value is expected to be higher. However, the increase in potassium ion concentration for the NT structure is only about  $0.33/0.12 \approx 2.8$  times that of the smooth structure (Fig. 4d). The simulation results shed light on the working mechanism of the Pt–Ni NTAs suggesting that

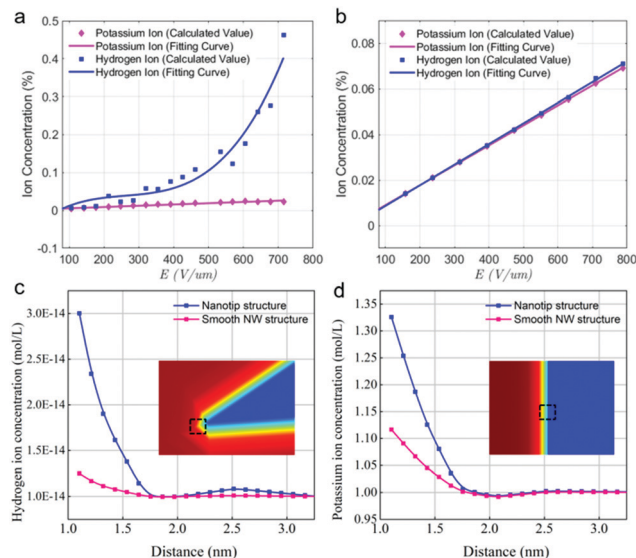


Fig. 4 Calculated ion concentration induced by the local electric field on the fabricated electrode. The calculated percentage of hydrogen and potassium ion concentration on the surface of (a) NT structure and (b) smooth NW model with  $2 \text{ nm}$  distance to the surface. The ion concentration % here represents the percentage of increased ion concentration on the electrode surface to the initial concentration. (c) The calculated hydrogen ion concentration and (d) the calculated potassium ion concentration at different distances to the electrode surface at  $350 \text{ V } \mu\text{m}^{-1}$ . Inset: The marked region highlights the calculated area.

the increased electric field intensity can modify the adsorption kinetics for different cations ( $\text{K}^+$  and  $\text{H}^+$ ). This behavior can be ascribed on the basis of electric field distribution on both surfaces. The induced electric field intensity is uniform in a smooth NW model and the difference between the electric field intensity at the calculated point and its surrounding point is very negligible, which can be attributed to an easier charge balance on the surface. In contrast to this, for the NT structure, the local electric field is distorted due to the presence of NT tips on the surface, which makes a substantial difference of electric field intensity at the calculated point with respect to its surroundings. Therefore, on this surface, ion movement is a little complex and cannot easily reach a charge balance. Furthermore, the dominant attraction of hydrogen ions is attributed to the faster diffusion rates as compared to potassium ions, due to the lighter weight of hydrogen ions, so they enrich the electrode surface rapidly in the presence of an induced electric field before the final charge balance is reached. Thus, the simulation analyses support experimental observations and explain the enhanced intrinsic activity caused by the high curvature nanotips. The fabricated Pt–Ni NTA structure offers a plethora of NT tips for large areal density ( $\sim 140$  per unit  $\mu\text{m}^{-2}$ ), which justifies the extremely low overpotential due to effective mass transfer of hydrogen ions on the catalyst surface in comparison with smooth NWs.

### 3 Conclusions

In summary, we demonstrate that our unique Pt distributed NT shaped nanostructure promotes selective accumulation of

H<sup>+</sup> around the cathode surface to enable a “pseudo acidic” local environment, which boosts the HER activity in alkaline solutions significantly. The optimized catalyst achieves an extremely small overpotential of 71 mV at a current density of 200 mA cm<sup>-2</sup>, which is the best alkaline HER activity among the ever-reported Pt-based catalysts at a current density of more than 100 mA cm<sup>-2</sup>, as far as we know. Its striking performance can be ascribed to the intriguing geometric and electronic structure which facilitates enhanced adsorption of hydrogen ions and fast bubble release from the electrode. Theoretical results demonstrate that a large area NT structure can increase the induced electric field on the tips, and thereby enhanced adsorption of hydrogen ions (~8 times higher) around the tips as compared to the smooth NW surface has been observed. Furthermore, optimizing the geometric characteristics of such NT structure and incorporating different elements can lead to more advanced catalytic electrodes for a variety of applications.

## Conflicts of interest

There are no conflicts to declare.

## Acknowledgements

The authors acknowledge financial support from the National Natural Science Foundation of China (No. 21950410512, 21875137, 51521004, 51420105009, 52061160482, 51950410577), Guangdong Province Science and Technology Department (Project No. 2020A0505100014), Shenzhen Environmental Science and New Energy Technology Engineering Laboratory (No. SDRC 2016172), AME Individual Research Grant (No. A1983c0026), Agency for Science, Technology, and Research (A\*STAR), Innovation Program of Shanghai Municipal Education Commission (No. 2019-01-07-00-02-E00069), and the 111 Project (No. B16032) for financial support. Adeela Nairan thanks Dr Dang Wu and Mr Jiaxing Liu for constructive discussions about the sample preparation techniques. Caiwu Liang thanks Mr Weisheng Pan for constructive discussions on electrochemical test.

## References

- 1 Y. Zheng, Y. Jiao, L. H. Li, T. Xing, Y. Chen, M. Jaroniec and S. Z. Qiao, *ACS Nano*, 2014, **8**, 5290–5296.
- 2 J. X. Feng, H. Xu, S. H. Ye, G. Ouyang, Y. X. Tong and G. R. Li, *Angew. Chem., Int. Ed.*, 2017, **56**, 8120–8124.
- 3 M. S. Dresselhaus and I. L. Thomas, *Nature*, 2001, **414**, 332–337.
- 4 J.-X. Feng, H. Xu, Y.-T. Dong, X.-F. Lu, Y.-X. Tong and G.-R. Li, *Angew. Chem., Int. Ed.*, 2017, **56**, 2960–2964.
- 5 S. Shima, O. Pilak, S. Vogt, M. Schick, M. S. Stagni, W. Meyer Klauke, E. Warkentin, R. K. Thauer and U. Ermler, *Science*, 2008, **321**, 572–575.
- 6 J.-X. Feng, S.-Y. Tong, Y.-X. Tong and G.-R. Li, *J. Am. Chem. Soc.*, 2018, **140**, 5118–5126.
- 7 J. K. Norskov and C. H. Christensen, *Science*, 2006, **312**, 1322–1323.
- 8 S. Bai, C. Wang, M. Deng, M. Gong, Y. Bai, J. Jiang and Y. Xiong, *Angew. Chem., Int. Ed.*, 2014, **53**, 12120–12124.
- 9 Q. Li, L. Wu, G. Wu, D. Su, H. Lv, S. Zhang, W. Zhu, A. Casimir, H. Zhu, A. Mendoza-Garcia and S. Sun, *Nano Lett.*, 2015, **15**, 2468–2473.
- 10 P. Wang, X. Zhang, J. Zhang, S. Wan, S. Guo, G. Lu, J. Yao and X. Huang, *Nat. Commun.*, 2017, **8**, 14580–14588.
- 11 A. J. M. Mackus, M. A. Verheijen, N. Leick, A. A. Bol and W. M. M. Kessels, *Chem. Mater.*, 2013, **25**, 1905–1911.
- 12 P. De Luna, R. Quintero-Bermudez, C.-T. Dinh, M. B. Ross, O. S. Bushuyev, P. Todorović, T. Regier, S. O. Kelley, P. Yang and E. H. Sargent, *Nat. Catal.*, 2018, **1**, 103–110.
- 13 T. Saberi Safaei, A. Mepham, X. Zheng, Y. Pang, C.-T. Dinh, M. Liu, D. Sinton, S. O. Kelley and E. H. Sargent, *Nano Lett.*, 2016, **16**, 7224–7228.
- 14 M. Liu, Y. Pang, B. Zhang, P. D. Luna, O. Voznyy, J. Xu, X. Zheng, C. T. Dinh, F. Fan, C. Cao, F. P. G. D. Arquer, T. S. Safaei, A. Mepham, A. Klinkova, E. Kumacheva, T. Filleter, D. Sinton, S. O. Kelley and E. H. Sargent, *Nature*, 2016, **537**, 382.
- 15 A. Guerrero-Martínez, S. Barbosa, I. Pastoriza-Santos and L. M. Liz-Marzán, *Curr. Opin. Colloid Interface Sci.*, 2011, **16**, 118–127.
- 16 K.-H. Choi, Y. Jang, D. Y. Chung, P. Seo, S. W. Jun, J. E. Lee, M. H. Oh, M. Shokouhimehr, N. Jung, S. J. Yoo, Y.-E. Sung and T. Hyeon, *Chem. Commun.*, 2016, **52**, 597–600.
- 17 Z. Peng and H. Yang, *Nano Today*, 2009, **4**, 143–164.
- 18 L. Liao, S. N. Wang, J. J. Xiao, X. J. Bian, Y. H. Zhang, M. D. Scanlon, X. L. Hu, Y. Tang and B. H. Liu, *Energy Environ. Sci.*, 2014, **7**, 387–392.
- 19 Y.-Y. Chen, Y. Zhang, X. Zhang, T. Tang, H. Luo, S. Niu, Z.-H. Dai, L.-J. Wan and J.-S. Hu, *Adv. Mater.*, 2017, **29**, 1703311.
- 20 J. Mahmood, F. Li, S.-M. Jung, M. S. Okyay, I. Ahmad, S.-J. Kim, N. Park, H. Y. Jeong and J.-B. Baek, *Nat. Nanotechnol.*, 2017, **304**, 1038.
- 21 S. Ye, F. Luo, Q. Zhang, P. Zhang, T. Xu, Q. Wang, D. He, L. Guo, Y. Zhang, C. He, X. Ouyang, M. Gu, J. Liu and X. Sun, *Energy Environ. Sci.*, 2019, **12**, 1000–1007.
- 22 C. Dong, C. Lian, S. Hu, Z. Deng, J. Gong, M. Li, H. Liu, M. Xing and J. Zhang, *Nat. Commun.*, 2018, **9**, 1252.
- 23 H. Li, S. Chen, Y. Zhang, Q. Zhang, X. Jia, Q. Zhang, L. Gu, X. Sun, L. Song and X. Wang, *Nat. Commun.*, 2018, **9**, 2452.
- 24 D. Liu, X. Li, S. Chen, H. Yan, C. Wang, C. Wu, Y. A. Haleem, S. Duan, J. Lu, B. Ge, P. M. Ajayan, Y. Luo, J. Jiang and L. Song, *Nat. Energy*, 2019, **4**, 512–518.
- 25 X. Yan, L. Tian, K. Li, S. Atkins, H. Zhao, J. Murowchick, L. Liu and X. Chen, *Adv. Mater. Interfaces*, 2016, **3**, 1600368.
- 26 Q. Sun, Y. Dong, Z. Wang, S. Yin and C. Zhao, *Small*, 2018, **14**, 1704137.